Journal of Alloys and Compounds 502 (2010) 68–73

Contents lists available at ScienceDirect

Journal of Alloys and Compounds

journal homepage: www.elsevier.com/locate/jallcom

Interaction of the components in the Ag–Er–Sn system at 400 °C

Jianlie Liang*, Changzhong Liao, Yiyuan Tang, Cailiu Yin, Yanmei Han, Liangqin Nong, Shibiao Xie

Institute of Materials Science, College of Physics and Electronic Engineering, Guangxi University for Nationalities, Nanning Guangxi 530006, PR China

ARTICLE INFO

Article history:
Received 22 February 2010
Received in revised form 7 April 2010
Accepted 22 April 2010
Available online 15 May 2010

Keywords:
Phase diagram
Ag–Er–Sn
X-ray diffraction
Scan electron microprobe

ABSTRACT

The phase equilibria in the Ag–Er–Sn ternary system at 400 °C were studied over the whole composition range by means of X-ray diffraction and scan electron microscope and energy dispersive X-ray spectroscopy. A new ternary compound with composition of $Er_{24.6}Ag_{18.9}Sn_{56.5}$, designed τ, and binary phase Er_3Sn_7 had been discovered. The Er_3Sn_7 phase adopts the Tb_3Sn_7 structure type with lattice constants of $a = 0.4377\ (1)$ nm, $b = 2.5578\ (9)$ nm and $c = 0.4333\ (2)$ nm. Other two ternary compounds, i.e., $AgErSn_2$ and AgErSn, were confirmed, too.

1. Introduction

Phase diagram is the "roadmap" for the materials design. Experimental data of the phase equilibria are fundamental for the materials design based on the CALPHAD method [1], and subsequent Phase Field Simulation [1,2]. Moreover, exploration on the phase diagram always accompanied the discovery of new intermetallics, which might be the potential functional materials. However, knowledge of the phase equilibria in some ternary alloys is incomplete and even scarce. As to the RE–Ag–Sn alloys, phase equilibria in the RE (RE = La, Ce, Pr, Nd, Gd, Dy, Yb) –Ag–Sn [3–9] have been reported in the form of isothermal section. Up to now, the phase equilibria in the Ag–Er–Sn system are not yet studied. To extend our knowledge of the RE–Ag–Sn alloys, we aim to determine the phase relationship of the Ag–Er–Sn system in this work.

Massalski [10] assessed the Er–Sn system mainly based on two incomplete phase diagrams established by Love [11] in composition range from 0 to 33.3 at.% Sn and Kulagina et al. [12] from 66.7 to 100 at.% Sn, respectively. According to Massalski [10], five intermetallic compounds formed in this system, i.e., Er_2Sn, Er_5Sn_3, $Er_{11}Sn_{10}$, $ErSn_2$ and $ErSn_3$. Palenzona and Manfrinetti [13] later identified the existence of Er_2Sn_5 when reinvestigating the Sn-rich part of this system. Except Er_2Sn, recent investigations on the Co–Er–Sn [14] and Cu–(Sm,Er)–Sn [15] ternary systems confirmed the existence of Er_5Sn_3, $Er_{11}Sn_{10}$, $ErSn_2$, Er_2Sn_5 and $ErSn_3$.

Three compounds exist in the Ag–Er system: AgEr, $AgEr_2$ and $Ag_{51}Er_{14}$ [16]. As regarding to the Ag–Sn binary system, two binary compounds, Ag_3Sn and Ag_4Sn, were reported [17].

Two ternary compounds were known for the Ag–Er–Sn system, i.e., AgErSn [18] and $AgErSn_2$ [19]. Table 1 summarized the crystallographic data of the binary boundary phases and ternary compounds in this system.

2. Experimental procedures

Fifty-five alloy buttons with the weight of 2 g each were prepared by arc-melting the pure elemental Ag (99.9 wt.%), Er (99.9 wt.%) and Sn (99.9 wt.%) under high purity argon atmosphere. To improve the homogeneity, each of the alloys were turned over and remelted for three times. Weight losses for the specimens range from about 1 to 1.5 wt%. No chemical analysis was carried out for the alloys. The ingots were then sealed in evacuated silica capsules, and annealed at 400 °C for 30 days. After completion of annealing, the samples were quenched in water with the tubes not broken.

X-ray diffraction (XRD) was performed with Rikagu-2500 diffractometer with CuKα operating at tube voltage of 40 kV and current of 250 mA. The lattice parameters were calculated by using the WinPLOTR program package [20]. Microstructural examination and composition microanalysis were carried out by using Hitachi 3400N scanning electron microscope (SEM) equipped with EDAX energy dispersive spectrometer (EDS).

3. Results and discussion

Table 2 summarizes the experimental results of XRD for the selected alloys. Those severely oxidized alloys are rejected in Table 2. Some off-equilibrium alloys were also collected in Table 2, as they substantiated the existence of some binary or ternary phases. Based on the data available in Table 2, the phase equilibria in Ag–Er–Sn are drawn in Fig. 1. Similar to other M(M = Cu, Ag, Au)–RE–Sn systems, the alloys within or close to the region

* Corresponding author. Tel.: +86 771 3260135; fax: +86 771 3261718.
E-mail address: jianlieliang@126.com (J. Liang).

0925-8388/$ – see front matter © 2010 Elsevier B.V. All rights reserved.
doi:10.1016/j.jallcom.2010.04.148

Table 1
Crystallographic data of already known binary boundary phases and ternary compounds in the Ag–Er–Sn system.

Phases	Space group	Pearson symbol	Prototype	Lattice parameters (nm)			References
				a	*b*	*c*	
$ErSn_3$[a]	$Pm\bar{3}m$	cP4	$AuCu_3$	0.4648 (2)			[18]
$ErSn_3$[b]	*Amm*2	oC16	$GdSn_{2.75}$	0.4336	0.4367	2.1685	[13]
Er_2Sn_5			Y_2Sn_5	0.4305	0.4391	1.8892	[13]
$ErSn_2$	*Cmcm*	oC12	$ZrSi_2$	0.4365 (2)	1.6132 (5)	0.4285 (2)	[18]
$Er_{11}Sn_{10}$	*I*4/*mmm*	tI84	$Ho_{11}Ge_{10}$	1.144		1.674	[18]
Er_5Sn_3	*P*63/*mcm*	hP16	Mn_5Si_3	0.8799		0.6442	[18]
AgEr	$Pm\bar{3}m$	cP2	CsCl	0.3574 (2)			[18]
Ag_2Er	*I*4/*mmm*	tI6	$MoSi_2$	0.3668 (1)		0.9159 (1)	[18]
$Ag_{51}Er_{14}$	*P*6/*m*	hP68	$Ag_{51}Gd_{14}$	1.24880		0.91730	[18]
Ag_3Sn	*Pmmn*	oP8	Cu_3Ti	0.47802 (4)	0.5968 (9)	0.51843 (9)	[18]
Ag_4Sn	*P*63/*mmc*	hP2	Mg	0.29658		0.47824	[18]
AgErSn	*P*63/*mmc*	hP6	$CaIn_2$	0.4661 (3)		0.7291 (5)	[18]
$AgErSn_2$	$Pm\bar{3}m$	cP4	$AuCu_3$	0.45344 (2)			[19]

[a] High temperature phase.
[b] Low temperature phase.

Table 2
Summary of experimental results of XRD for the selected alloys.

	Nominal composition (at.%)			Phase identified by XRD	Space group	Structure type	Lattice parameters (nm)
	Sn	Ag	Er				
1	65	25	10	Er_3Sn_7	*Cmmm*	Tb_3Sn_7	$a = 0.4377(1)$, $b = 2.5578(9)$, $c = 0.4333(2)$
				Liquid [(Sn) + Ag_3Sn]			
2[a]	35	50	15	$AgErSn_2$	$Pm\bar{3}m$	$AuCu_3$	$a = 0.45048(1)$
				AgErSn	*P*63/*mmc*	$CaIn_2$	$a = 0.46438(3)$, $c = 0.72492(7)$
				Ag_3Sn	*Pmmn*	Cu_3Ti	$a = 0.4769(2)$, $b = 0.5952(3)$, $c = 0.5185(3)$
				τ	Structure unknown	Trace	
3	25	60	15	AgErSn	*P*63/*mmc*	$CaIn_2$	$a = 0.46583(1)$, $c = 0.72946(2)$
				Ag_4Sn	*P*63/*mmc*	Mg	$a = 0.29689(2)$, $c = 0.47859(7)$
4	10	70	20	AgErSn	*P*63/*mmc*	$CaIn_2$	$a = 0.46645(3)$, $c = 0.72939(6)$
				(Ag)	$Fm\bar{3}m$	Cu	$a = 0.40883(2)$
				$Ag_{51}Er_{14}$	*P*6/*m*	$Ag_{51}Gd_{14}$	$a = 1.2541(1)$, $c = 0.9244(1)$
5	15	55	30	AgErSn	*P*63/*mmc*	$CaIn_2$	$a = 0.46622(1)$, $c = 0.72845(3)$
				$Ag_{51}Er_{14}$	*P*6/*m*	$Ag_{51}Gd_{14}$	$a = 1.25906(8)$, $c = 0.92222(7)$
6	10	50	40	Er_5Sn_3	*P*63/*mcm*	Mn_5Si_3	
				Ag_2Er	*I*4/*mmm*	$MoSi_2$	
7	20	30	50	Er_5Sn_3	*P*63/*mcm*	Mn_5Si_3	$a = 0.88086(4)$, $c = 0.64392(3)$
				Ag_2Er	*I*4/*mmm*	$MoSi_2$	$a = 0.36689(4)$, $c = 0.9158(1)$
				AgEr	$Pm\bar{3}m$	CsCl	Trace
8	20	15	65	Er_5Sn_3	*P*63/*mcm*	Mn_5Si_3	$a = 0.88132(2)$, $c = 0.64474(1)$
				AgEr	$Pm\bar{3}m$	CsCl	$a = 0.35841(2)$
				(Er)	*P*63/*mmc*	Mg	$a = 0.35707(5)$, $c = 0.55988(3)$
9	10	20	70	Er_5Sn_3	*P*63/*mcm*	Mn_5Si_3	$a = 0.87992(3)$, $c = 0.64340(2)$
				AgEr	$Pm\bar{3}m$	CsCl	$a = 0.35787(2)$
				(Er)	*P*63/*mmc*	Mg	$a = 0.35667(3)$, $c = 0.56116(7)$
10	50	15	35	AgErSn	*P*63/*mmc*	$CaIn_2$	$a = 0.46624(1)$, $c = 0.72912(2)$
				$ErSn_2$	*Cmcm*	$ZrSi_2$	$a = 0.43684(2)$, $b = 1.61224(8)$, $c = 0.42853(2)$
				$AgErSn_2$	$Pm\bar{3}m$	$AuCu_3$	$a = 0.45156(1)$
11	48	20	32	AgErSn	*P*63/*mmc*	$CaIn_2$	$a = 0.46631(1)$, $c = 0.72916(2)$
				$ErSn_2$	*Cmcm*	$ZrSi_2$	$a = 0.43692(2)$, $b = 1.61277(9)$, $c = 0.42880(2)$
				$AgErSn_2$	$Pm\bar{3}m$	$AuCu_3$	$a = 0.45155(1)$
12	51	20	29	AgErSn	*P*63/*mmc*	$CaIn_2$	$a = 0.46607(4)$, $c = 0.7276(1)$
				$ErSn_2$	*Cmcm*	$ZrSi_2$	Trace
				$AgErSn_2$	$Pm\bar{3}m$	$AuCu_3$	$a = 0.45171(9)$
13	55	17	28	$AgErSn_2$	$Pm\bar{3}m$	$AuCu_3$	$a = 0.45297(6)$
				$ErSn_2$	*Cmcm*	$ZrSi_2$	Trace, not determined
14	61	10	29	$AgErSn_2$	$Pm\bar{3}m$	$AuCu_3$	$a = 0.45379(1)$
				$ErSn_2$	*Cmcm*	$ZrSi_2$	$a = 0.43623(2)$, $b = 1.61152(9)$, $c = 0.42815(2)$
15[a]	63	10	27	$AgErSn_2$	$Pm\bar{3}m$	$AuCu_3$	$a = 0.45279(2)$
				$ErSn_2$	*Cmcm*	$ZrSi_2$	$a = 0.43584(3)$, $b = 1.6099(1)$, $c = 0.42781(3)$
				Er_3Sn_7	*Cmmm*	Tb_3Sn_7	$a = 0.43842(4)$, $b = 2.5414(2)$, $c = 0.43394(4)$
				(Sn)	$I4_1/amd$	Sn	$a = 0.58192(2)$, $c = 0.31684(1)$
				Ag_3Sn	*Pmmn*	Cu_3Ti	$a = 0.4776(2)$, $b = 0.5974(3)$, $c = 0.5194(2)$
16[b]	70	10	20	Er_2Sn_5	*Pmmn*	Er_2Ge_5	$a = 0.4298(2)$, $b = 0.4389(2)$, $c = 1.8867(5)$
				Er_3Sn_7	*Cmmm*	Tb_3Sn_7	$a = 0.4376(1)$, $b = 2.5534(1)$, $c = 0.4330(1)$
				(Sn)	$I4_1/amd$	Sn	$a = 0.58303(2)$, $c = 0.31818(1)$
				Ag_3Sn	*Pmmn*	Cu_3Ti	$a = 0.4803(3)$, $b = 0.5965(1)$, $c = 0.5190(3)$
17	45	10	45	AgErSn	*P*63/*mmc*	$CaIn_2$	$a = 0.46609(2)$, $c = 0.72931(4)$
				$ErSn_2$	*Cmcm*	$ZrSi_2$	$a = 0.43705(4)$, $b = 1.6129(2)$, $c = 0.42885(4)$
				$Er_{10}Sn_{11}$?	*I*4/*mmm*	$Ho_{11}Ge_{10}$	

Table 2(*Continued*)

	Nominal composition (at.%)			Phase identified by XRD	Space group	Structure type	Lattice parameters (nm)
	Sn	Ag	Er				
18	73	0	27	Er_2Sn_5	*Pmmn*	Er_2Ge_5	$a=0.43007(5)$, $b=0.43741(5)$, $c=1.8872(3)$
				(Sn)	$I4_1/amd$	Sn	$a=0.58257(2)$, $b=0.31799(1)$
19	70	0	30	Er_2Sn_5	*Pmmn*	Er_2Ge_5	$a=0.43001(4)$, $b=0.43746(4)$, $c=1.8871(2)$
				$ErSn_2$	*Cmcm*	$ZrSi_2$	
20	0	50	50	$Er_{11}Sn_{10}$	*I4/mmm*	$Ho_{11}Ge_{10}$	
				$ErSn_2$	*Cmcm*	$ZrSi_2$	
21	57	5	38	$AgErSn_2$	$Pm\bar{3}m$	$AuCu_3$	
				$ErSn_2$	*Cmcm*	$ZrSi_2$	
22	30	20	50	Er_5Sn_3	*P63/mcm*	Mn_5Si_3	$a=0.8802(5)$, $c=0.6502(3)$
				AgErSn	*P63/mmc*	$CaIn_2$	$a=0.4668(6)$, $c=0.7302(8)$
				Ag_2Er ?	*I4/mmm*	$MoSi_2$	Trace
23	40	32	28	AgErSn	*P63/mmc*	$CaIn_2$	$a=0.46631(1)$, $c=0.72919(2)$
				Ag_3Sn	*Pmmn*	Cu_3Ti	$a=0.4783(2)$, $b=0.5959(2)$, $c=0.5179(2)$
				$AgErSn_2$	$Pm\bar{3}m$	$AuCu_3$	$a=0.45078(1)$
24	40	40	20	AgErSn	*P63/mmc*	$CaIn_2$	$a=0.46656(2)$, $c=0.72962(2)$
				Ag_3Sn	*Pmmn*	Cu_3Ti	$a=0.47946(7)$, $b=0.59178(9)$, $c=0.51509(8)$
				$AgErSn_2$	$Pm\bar{3}m$	$AuCu_3$	$a=0.45164(1)$
25	30	45	25	AgErSn	*P63/mmc*	$CaIn_2$	$a=0.46638(1)$, $c=0.72932(2)$
				Ag_3Sn	*Pmmn*	Cu_3Ti	$a=0.47805(9)$, $b=0.5973(2)$, $c=0.5186(2)$
26	10	40	50	Ag_2Er	*I4/mmm*	$MoSi_2$	
				Er_5Sn_3	*P63/mcm*	Mn_5Si_3	
27[b]	65	20	15	Er_3Sn_7	*Cmmm*	Tb_3Sn_7	
				τ	Structure unknown		
				Ag_3Sn	*Pmmn*	Cu_3Ti	
				(Sn)	$I4_1/amd$	Sn	
28[b]	60	20	20	τ	Structure unknown		
				Ag_3Sn	*Pmmn*	Cu_3Ti	
				(Sn)	$I4_1/amd$	Sn	
29[b]	65	15	20	Er_3Sn_7	*Cmmm*	Tb_3Sn_7	$a=0.43758(1)$, $b=2.5540(9)$, $c=0.43306(1)$
				Ag_3Sn	*Pmmn*	Cu_3Ti	$a=0.4813(6)$, $b=0.5948(5)$, $c=0.5193(5)$
				(Sn)	$I4_1/amd$	Sn	$a=0.58322(2)$, $c=0.31816(1)$
30[b]	58	20	22	τ	Structure unknown		
				Ag_3Sn	*Pmmn*	Cu_3Ti	
				(Sn)	$I4_1/amd$	Sn	
31[b]	60	15	25	Er_3Sn_7	*Cmmm*	Tb_3Sn_7	
				τ	Structure unknown		
				Ag_3Sn	*Pmmn*	Cu_3Ti	
				(Sn)	$I4_1/amd$	Sn	
32[b]	52	28	20	τ	Structure unknown		
				Ag_3Sn	*Pmmn*	Cu_3Ti	
				(Sn)	$I4_1/amd$	Sn	
33	14	62	24	AgErSn	*P63/mmc*	$CaIn_2$	$a=0.46637(3)$, $c=0.72800(6)$
				(Ag)	$Fm\bar{3}m$	Cu	$a=0.40861(2)$
				$Ag_{51}Er_{14}$	*P6/m*	$Ag_{51}Gd_{14}$	$a=1.2578(1)$, $c=0.9221(1)$
34	23	46	31	AgErSn	*P63/mmc*	$CaIn_2$	$a=0.46604(2)$, $c=0.72797(4)$
				(Ag)	$Fm\bar{3}m$	Cu	$a=0.4020(2)$
				$Ag_{51}Er_{14}$	*P6/m*	$Ag_{51}Gd_{14}$	$a=1.2564(3)$, $c=0.9235(3)$
35	52	26	22	τ	Structure unknown		
				Ag_3Sn	*Pmmn*	Cu_3Ti	
36	65	0	35	$ErSn_2$	*Cmcm*	$ZrSi_2$	$a=0.43579(6)$, $b=1.6108(2)$, $c=0.4275(6)$
				(Sn)	$I4_1/amd$	Sn	$a=0.58308(3)$, $c=0.31817(1)$
37[b]	55	20	25	τ	Structure unknown		
				Ag_3Sn	*Pmmn*	Cu_3Ti	
				(Sn)	$I4_1/amd$	Sn	
38[b]	55	22	23	τ	Structure unknown		
				Ag_3Sn	*Pmmn*	Cu_3Ti	
				(Sn)	$I4_1/amd$	Sn	
39[b]	55	18	27	τ	Structure unknown		
				Ag_3Sn	*Pmmn*	Cu_3Ti	
				(Sn)	$I4_1/amd$	Sn	
40	50	25	25	$AgErSn_2$	$Pm\bar{3}m$	$AuCu_3$	$a=0.45095(7)$

[a] The alloys are off-equilibrium.
[b] Ag_3Sn and (Sn) in these alloys resulted from the solidification of liquid during the quench.

of Er_5Sn_3 to $Er_{11}Sn_{10}$ were found sensitive to moisture and oxygen and were readily discarded. For this reason, we could not observe $Er_{11}Sn_{10}$ in the ternary alloys. Thus, the $Er_{11}Sn_{10}$ related tie-triangles are connected with dot line. Single $AgErSn_2$ phase was obtained in alloy 40 ($Ag_{25}Er_{25}Sn_{50}$), and its lattice parameter was calculated to be $a=0.45095(7)$ nm. For $AgErSn_2$, its lattice constant was found significant change in alloys 11–14 with the variation of the alloys' composition. The fact implies that there is a small homogeneity for this compound. $Ag_{51}Er_{14}$ and liquid should occupy a certain area considering the adjacent phase relationships. However, no the effort was made to measure the phase boundaries of $AgErSn_2$ as well as $Ag_{51}Er_{14}$ and liquid. Thus, the boundaries of these phases were drawn tentatively in Fig. 1. To support the proposed tie triangles, Figs. 2–5 present XRD results of several equilibrated alloys.

In the present work, a new ternary compound, designed τ, was found and identified. Fig. 6 presents the XRD results of alloys 28

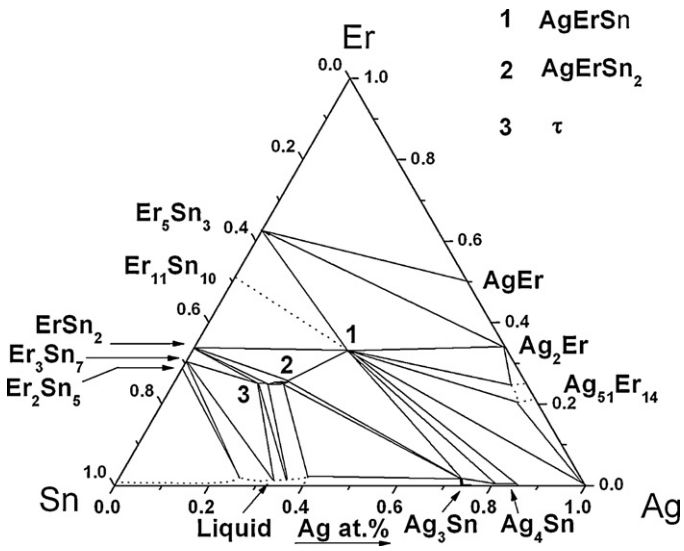

Fig. 1. Phase equilibria of the Ag–Er–Sn ternary system at 400 °C. The boundaries of $AgErSn_2$ and liquid phase and $Ag_{51}Er_{14}$ are tentative.

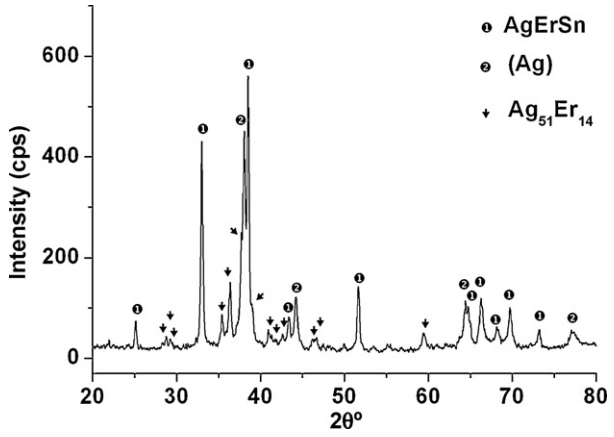

Fig. 2. XRD result of alloy 4 annealed at 400 °C for 30 days, showing the co-existence of AgErSn and (Ag) and $Ag_{51}Er_{14}$.

($Ag_{20}Er_{20}Sn_{60}$), 30 ($Ag_{20}Er_{22}Sn_{58}$) and 32 ($Ag_{28}Er_{20}Sn_{52}$), where the intense peaks labeled in full circle were identified as τ. The peak positions in two-theta attributed to this new ternary compound are listed as follows: 34.20°, 36.45°, 41.26°, 56.27°, 59.83°, 64.28°, 70.80° and 72.17°. However, except (Sn) and Ag_3Sn, there are many

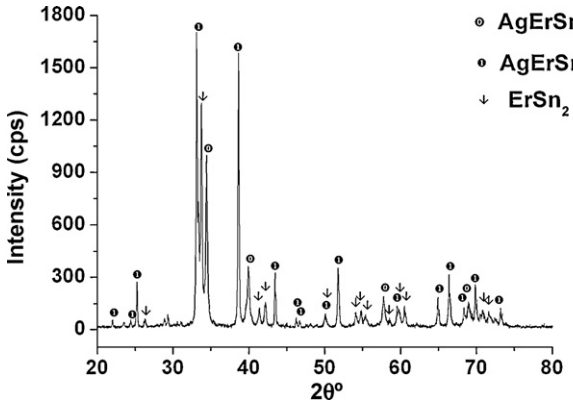

Fig. 3. XRD result of alloy 11 annealed at 400 °C for 30 days, showing the co-existence of $AgErSn_2$ and AgErSn and $ErSn_2$.

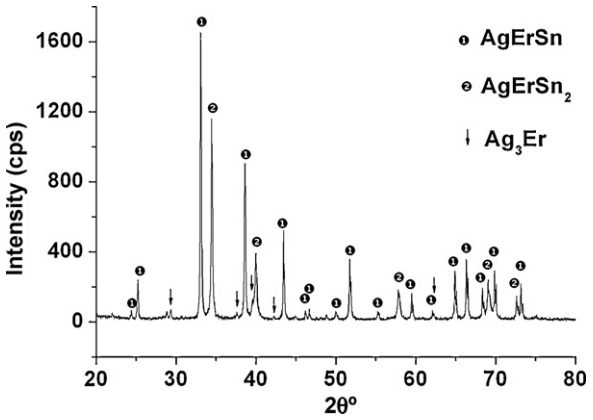

Fig. 4. XRD result of alloy 23 annealed at 400 °C for 30 days, showing the co-existence of $AgErSn_2$ and AgErSn and Ag_3Sn.

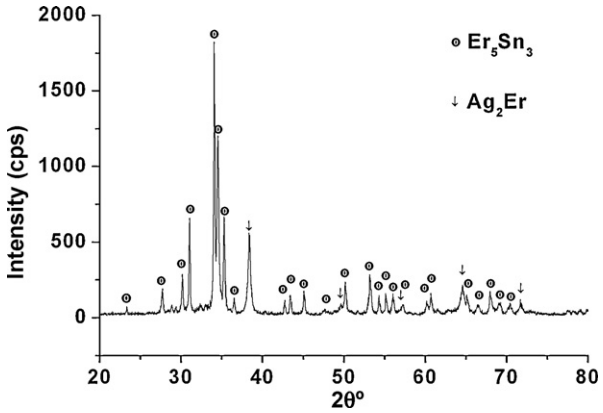

Fig. 5. XRD result of alloy 7 annealed at 400 °C for 30 days, showing the co-existence of Ag_2Er and Er_5Sn_3.

unidentified weak peaks in Fig. 6. To clarify the composition of this new ternary compound, alloy 32 ($Ag_{28}Er_{20}Sn_{52}$) was subjected to SEM/EDS examination. Matrix τ phase and Ag_3Sn and (Sn) were observed in this alloy. The composition of τ was measured to be of 24.6 at.% Ag, 18.9 at.% Er and 56.5 at.% Sn, while that of Ag_3Sn was 73.6 at.% Ag, 1.1 at.% Er and 25.3 at.% Sn. In order to synthesize this compound, several other alloys, such as alloys 37 ($Ag_{20}Er_{25}Sn_{55}$), 38 ($Ag_{20}Er_{27}Sn_{53}$) and 39 ($Ag_{18}Er_{27}Sn_{55}$), were melted and annealed

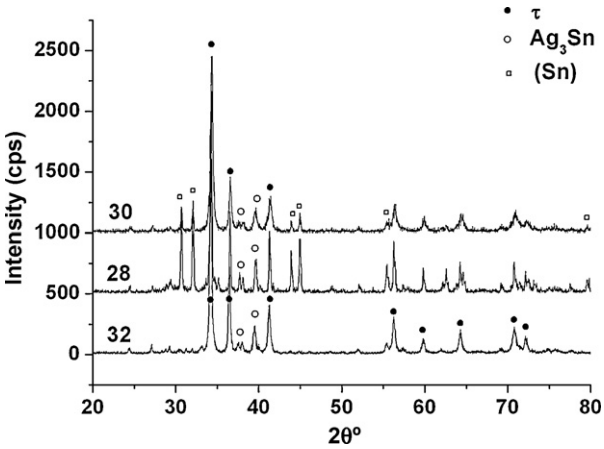

Fig. 6. The XRD results of alloys 28 ($Ag_{20}Er_{20}Sn_{60}$), 30 ($Ag_{20}Er_{22}Sn_{58}$) and 32 ($Ag_{28}Er_{20}Sn_{52}$). Except those of (Sn) and Ag_3Sn, peaks labeled in full circle were identified as to the new ternary compound τ.

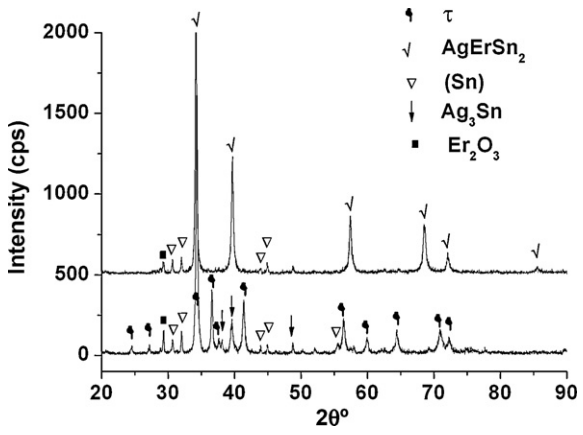

Fig. 7. XRD patterns of alloy 37 ($Ag_{20}Er_{25}Sn_{55}$) annealed at 400 and 500 °C, respectively.

at 400 °C for 7 days. Due to the segregation of (Sn), we failed to obtain single ternary compound τ.

The new ternary compound τ was found to disappear when the alloy was annealed at 500 °C for 7 days followed by water quenching. Fig. 7 compares the XRD results of alloy 37 ($Ag_{20}Er_{25}Sn_{55}$) heated at 400 and 500 °C, respectively. As shown in Fig. 7, new ternary phase τ and (Sn) and Ag_3Sn as well as trace amount of Er_2O_3 co-exist in the alloy heated at 400 °C. When temperature rises to 500 °C, Ag_3Sn and those peaks attributed to the new ternary compound as well as the unknown weak peaks vanished with the formation of $AgErSn_2$. This fact suggested that those unknown weak peaks mentioned above might belong to τ phase, as shown in Fig. 7.

X-ray patterns similar to Tb_3Sn_7 were observed in several ternary alloys, which implied that Er_3Sn_7 might form in the Er–Sn side. Fig. 8 presents the XRD results of alloys 1 ($Ag_{25}Er_{10}Sn_{65}$) and 16 ($Ag_{10}Er_{20}Sn_{70}$), where the peaks labeled in full circle are attributed to Er_3Sn_7. By assuming Er_3Sn_7 isostructural to Tb_3Sn_7, fair agreement in the calculated and observed peak intensities was obtained. Therefore, Er_3Sn_7 was believed to exist in the Er–Sn system. This conclusion is in contradiction to the results of Palenzona and Manfrinetti [13], in which RE_3Sn_7 type phases were excluded in (Er, Ho, Tm, Lu)–Sn systems but included in (Gd, Tb, Dy, Y)–Sn systems. The cell parameters of Er_3Sn_7 are calculated to be $a = 0.4377\ (1)$ nm, $b = 2.5578\ (9)$ nm and $c = 0.4333\ (2)$ nm in alloy 1 ($Ag_{25}Er_{10}Sn_{65}$). As shown in Fig. 8, alloy 16 ($Ag_{10}Er_{20}Sn_{70}$)

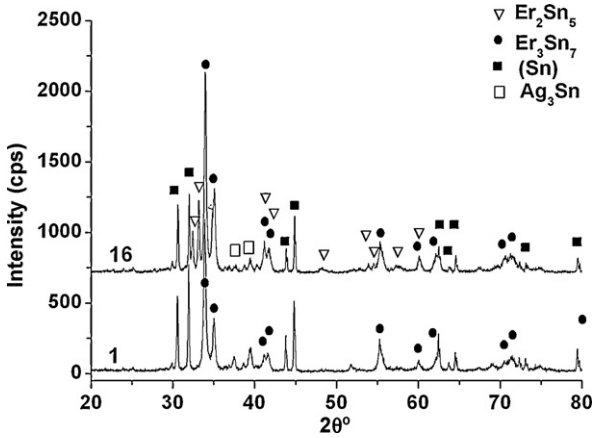

Fig. 8. The XRD results of alloys 16 ($Ag_{10}Er_{20}Sn_{70}$) and 1 ($Ag_{25}Er_{10}Sn_{65}$) annealed at 400 °C for 30 days followed by water quenching. Alloy 16 ($Ag_{10}Er_{20}Sn_{70}$) is composed of Er_2Sn_5, Er_3Sn_7, Ag_3Sn and (Sn), while alloy 1 ($Ag_{25}Er_{10}Sn_{65}$) consists of Er_3Sn_7, Ag_3Sn and (Sn). The latter two phases are the liquid products during the solidification.

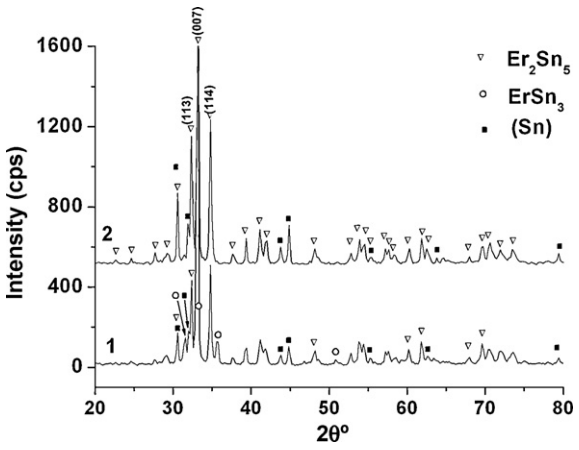

Fig. 9. XRD results of alloy 18 ($Er_{27}Sn_{73}$) annealed at (1) 700 °C for 30 days and (2) further annealed at 400 °C for 7 days.

is composed of Er_2Sn_5, Er_3Sn_7, Ag_3Sn and (Sn), while alloy 1 ($Ag_{25}Er_{10}Sn_{65}$) consists of Er_3Sn_7, Ag_3Sn and (Sn). The latter two phases are the liquid products during the solidification.

Alloys 18 ($Er_{27}Sn_{73}$) and 19 ($Er_{30}Sn_{70}$) were prepared to verify the existence of Er_2Sn_5. Er_3Sn_7 was thought to form through peritectic reaction at a temperature higher than that of Er_2Sn_5. Alloy 19 was expected to consist of single Er_3Sn_7 or ($Er_3Sn_7 + Er_2Sn_5$), if the practical composition of alloy only slightly deviated from the nominal composition. Thus, a higher annealing temperature 700 °C was arbitrarily chosen for these two alloys for the first time. Apart from Er_2Sn_5 and Sn, XRD detected additional trace amount of $ErSn_2$ for alloy 19 ($Er_{30}Sn_{70}$) and orthorhombic $ErSn_3$ for alloy 18 ($Er_{27}Sn_{73}$), after annealed at 700 °C for 30 days followed by air-cooling. When both alloys were re-heated at 400 °C for 7 days and followed by water quenching, alloy 19 ($Er_{30}Sn_{70}$) was observed to consist of Er_2Sn_5 and $ErSn_2$ with (Sn) almost vanished, while alloy 18 ($Er_{27}Sn_{73}$) consisted of Er_2Sn_5 and (Sn) with $ErSn_3$ thoroughly disappeared. Fig. 9 presents the XRD results of alloy 18 ($Er_{27}Sn_{73}$). Er_2Sn_5 was reported to adopt the Y_2Sn_5 crystal structure [13]. However, we could not find the crystal structural data of Y_2Sn_5 in the public literature. Recently, Venturini et al. determined the crystal structure of Er_2Ge_5 (space group, *Pmmn*) [21]. We thought that Er_2Sn_5 might be isostructural to Er_2Ge_5. Thus, substituting Sn into the positions of Ge, the XRD pattern of Er_2Sn_5 was calculated by using the Powdercell program [22]. Comparing the calculated patterns, Er_2Sn_5 was found to show strong preferred orientation in all the investigated alloys. As shown in Fig. 9, the (0 0 7) peak was observed to be the most intense while the theoretical strongest peak (1 1 3) to be the third intense.

Palenzona and Manfrinetti [13] indicated that the RSn_2 compounds showed very high stability, and could not be destroyed by annealing treatment unless remelting the alloy. This suggestion might be right for the binary alloys. However, for the ternary alloys, the suggestion might be questionable. In the present work, $ErSn_2$ and cubic-$AgErSn_2$ as well as (Sn) and Ag_3Sn were observed in the as-cast alloy 28 ($Ag_{20}Er_{20}Sn_{60}$). When this alloy is subjected to annealing at 400 °C for 20 days, $ErSn_2$ and cubic-$AgErSn_2$ vanished and the new ternary compound τ formed.

4. Conclusions

Phase equilibria of the Ag–Er–Sn ternary system were determined. Two new compounds, i.e., Er_3Sn_7 and τ, were identified for the first time. The Er_3Sn_7 phase crystallizes in Tb_3Sn_7 structure type with cell parameters of $a = 0.4377\ (1)$ nm, $b = 2.5578\ (9)$ nm

and $c = 0.4333\ (2)$ nm. The compositions of τ were measured to be of 24.6 at.% Ag, 18.9 at.% Er and 56.5 at.% Sn.

Acknowledgements

Financial supports from the Guangxi Science Foundation (Contract Nos. 0448022, 0542009 and 0640040), and Guangxi Large Scale Apparatus Corporation Office are greatly appreciated.

References

[1] Z.K. Liu, L.Q. Chen, P. Raghavan, Q. Du, J.O. Sofo, S.A. Langer, C. Wolverton, J. Comput. Aided Mater. Des. 11 (2004) 183–199.
[2] J.Z. Zhu, Z.K. Liu, V. Vaithyanathan, L.Q. Chen, Scripta Mater. 46 (2002) 401–406.
[3] J. Liang, C. Lian, Y. Du, Y. Tang, Y. Han, Y. He, S. Liu, J. Alloys Compd. 493 (2010) 122–127.
[4] P. Boulet, D. Mazzone, H. Noël, P. Riani, P. Rogl, R. Ferro, Intermetallics 7 (1999) 931–935.
[5] D. Mazzone, P. Riani, G. Zanicchi, R. Marazza, R. Ferro, Intermetallics 10 (2002) 801–809.
[6] P. Salamakha, O. Zaplatynsky, O. Sologub, O. Bodak, J. Alloys Compd. 239 (1996) 94–97.
[7] J.L. Liang, Y. Du, Y.Y. Tang, C.Z. Liao, J.L. Meng, H.H. Xu, J. Alloys Compd. 481 (2009) 264–269.
[8] V.V. Romaka, A. Tkachuk, V. Davydov, J. Alloys Compd. 439 (2007) 128–131.
[9] G. Zanicchi, D. Mazzone, P. Riani, R. Marazza, R. Ferro, J. Alloys Compd. 317–318 (2001) 513–520.
[10] T.B. Massalski, Binary Alloy Phase Diagrams, 2nd ed., ASM International, Metals Park, OH, 1990.
[11] B. Love, WADD Tech. Rep. 60–74, 1960, p. 226.
[12] I.G. Kulagina, A.P. Bayanov, N.M. Kulagin, Izv. Akad. Nauk SSSR, Met. 3 (1985) 211–216 (in Russian).
[13] A. Palenzona, P. Manfrinetti, J. Alloys Compd. 201 (1993) 43–47.
[14] R.V. Skolozdra, Ya.S. Mudryk, L.P. Romaka, J. Alloys Compd. 296 (2000) 290–292.
[15] I.V. Senkovska, Ya.S. Mudryk, L.P. Romaka, O.I. Bodak, J. Alloys Compd. 312 (2000) 124–129.
[16] K.A. Gschneidner, F.W. Calderwood, J. Phase Equilibr. 6 (1985) 17–19.
[17] I. Karakaya, W.T. Thompson, J. Phase Equilibr. 8 (1987) 340–347.
[18] P. Villar, Pearson's Handbook, Desk ed., ASM International, Materials Park, OH, 1997.
[19] V.V. Romaka, V. Davydov, L. Romaka, Yu. Stadnyk, J. Alloys Compd. 457 (2008) 329–331.
[20] T. Roisel, J. Rodriguez-Carvajal, WinPLOTR: A windows tool for powder diffraction patterns analysis, http://www-llb.cea.fr/fullweb/winplotr/winplotr.htm.
[21] G. Venturini, I. Ijjaali, B. Malaman, J. Alloys Compd. 288 (1999) 183–187.
[22] W. Krau, G. Nolze, Powdercell, Available in: http://www.ccp14.ac.uk/ccp/web-mirrors/powdcell/a_v/v_1/powder/e_cell.html.